Identifying underlying patterns in Alzheimer's disease trajectory: a deep learning approach and Mendelian randomization analysis

Fan Yi,[a,e] Yaoyun Zhang,[b,e] Jing Yuan,[c,e] Ziyue Liu,[c] Feifei Zhai,[c] Ankai Hao,[a] Fei Wu,[a] Judith Somekh,[d] Mor Peleg,[d] Yi-Cheng Zhu,[c,**] and Zhengxing Huang,[a,*] for the Alzheimer's Disease Neuroimaging Initiatives

[a]College of Computer Science and Technology, Zhejiang University, China
[b]DAMO Academy, Alibaba Group, China
[c]Department of Neurology, Peking Union Medical College Hospital, Peking Union Medical College, Chinese Academy of Medical Sciences, Beijing, 100730, China
[d]Department of Information Systems, University of Haifa, Haifa, Israel

eClinicalMedicine 2023;64: 102247
Published Online xxx
https://doi.org/10.1016/j.eclinm.2023.102247

Summary

Background Alzheimer's disease (AD) is a heterogeneously progressive neurodegeneration disorder with varied rates of deterioration, either between subjects or within different stages of a certain subject. Estimating the course of AD at early stages has treatment implications. We aimed to analyze disease progression to identify distinct patterns in AD trajectory.

Methods We proposed a deep learning model to identify underlying patterns in the trajectory from cognitively normal (CN) to a state of mild cognitive impairment (MCI) to AD dementia, by jointly predicting time-to-conversion and clustering out distinct subgroups characterized by comprehensive features as well as varied progression rates. We designed and validated our model on the ADNI dataset (1370 participants). Prediction of time-to-conversion in AD trajectory was used to validate the expression of the identified patterns. Causality between patterns and time-to-conversion was further inferred using Mendelian randomization (MR) analysis. External validation was performed on the AIBL dataset (233 participants).

Findings The proposed model clustered out patterns characterized by significantly different biomarkers and varied progression rates. The discovered patterns also showed a strong prediction ability, as indicated by hazard ratio (CN→MCI, HR = 3.51, $p < 0.001$; MCI→AD, HR = 8.11, $p < 0.001$), C-Index (CN→MCI, 0.618; MCI→AD, 0.718), and AUC (CN→MCI, 3 years 0.802, 5 years 0.876; MCI→AD, 3 years 0.914, 5 years 0.957). In the external validation cohort, our model demonstrated competitive performance on conversion time prediction (CN→MCI, C-Index = 0.693; MCI→AD, C-Index = 0.752). Moreover, suggestive associations between CN→MCI/MCI→AD patterns with four/three SNPs were mediated and MR analysis indicated a causal link between MCI→AD patterns and time-to-conversion in the first three years.

Interpretation Our proposed model identifies biologically and clinically meaningful patterns from real-world data and provides promising performance on time-to-conversion prediction in AD trajectory, which could promote the understanding of disease progression, facilitate clinical trial design, and provide potential for decision-making.

Funding The National Key Research and Development Program of China, the Key R&D Program of Zhejiang, and the National Nature Science Foundation of China.

Keywords: Alzheimer's disease; Progression pattern; Deep learning; Time-to-conversion prediction; Mendelian randomization

*Corresponding author.
**Corresponding author.
E-mail addresses: zhengxinghuang@zju.edu.cn (Z. Huang), zhuyc@pumch.cn (Y.-C. Zhu).
[e]Equal contribution to this article.

Research in context

Evidence before this study

Alzheimer's disease (AD), as the most common neurodegenerative disorder, is essentially heterogenous in its underlying progression trajectory. Deep learning-based methods have recently been proposed to unravel the heterogeneous mechanisms of AD by identifying distinct patterns in AD trajectory. We searched PubMed for articles published until December 31, 2022, using the search terms ["deep learning" OR "machine learning" OR "artificial intelligence"] AND ["Alzheimer's disease" OR "AD"] AND ["progression" OR "trajectory"] AND ["pattern" OR "subtype"]. We found that several studies had sought to uncover the phenotypic heterogeneity by using deep learning approaches to infer the disease subtypes and/or stages. However, a critical limitation of existing models is that they neglected the individualized differences of time-to-conversion to mild cognitive impairment (MCI)/AD dementia. In clinical reality, heterogeneous patients with AD may have varied rates of disease progression and may exhibit distinct patterns in their clinical biomarkers and neuroimaging features.

Added value of this study

This study aims to address the limitations of existing studies by simultaneously modeling clinical biomarkers, neuroimaging features and their temporal differences in trajectories of individualized patients with AD, using a deep learning-based survival clustering model. We trained and validated our model using clinical and T1-weighted MRI data of 1370 participants from the ADNI cohort, and externally validated our model in the AIBL cohort (233 participants). We showed the effectiveness of our model in identifying biologically and clinically meaningful patterns in AD trajectories. Time-to-conversion prediction was also conducted to demonstrate the prognostic power of the identified patterns. Moreover, potential causal link between the identified patterns and progression of AD was revealed by using Mendelian randomization analysis.

Implications of all the available evidence

The proposed model shows its effectiveness and generalizability in disentangling the underlying heterogeneity in AD trajectory, and clinical utility in predicting individual patient's time-to-conversion to MCI/AD dementia. Our study provides an effective tool for patient stratification and early prognosis of AD dementia, and to potentially facilitate subject screening in clinical trials.

Introduction

Alzheimer's disease (AD) is a neurodegenerative disorder with an insidious onset and progressive impairment of behavioral and cognitive functions, eventually leading to dementia.[1] Understanding AD progression is of great clinical significance.[2] While the clinical syndromic classification framework defined AD as the transition from a cognitively normal (CN) to a state of mild cognitive impairment (MCI) to AD dementia, the progression of between these stages is highly variable, with some patients showing stable cognitive function over time, whereas others progress rapidly. Over the past decades, a diversity of studies using mathematical functions attempted to portray the roadmap of disease progression in order to provide a personalized approach for disease management.[3–5] However, these works make a hard assumption that the rate of deterioration was homogeneous, either between subjects or within different stages of a certain subject, which is a fundamental problem.[6] To address the heterogeneity of AD, various deep learning methods, have been developed to try to reveal the underlying characteristics and patterns of AD[7–13] or provide time-to-conversion prediction for the progression of AD,[14–16] offering a great potential for early detection and prognosis of AD.

Understanding of heterogeneous disease progression should not only stand on cross-sectional modeling, but rather also recognize, analyze, and classify trajectories of patients with AD; however, this task is often hampered by lacking longitudinal data. Although machine learning algorithms, particularly deep learning tactics, can address the heterogeneous progression of AD and alleviate this problem by either concatenating multiple sectional data of different patients[17] or generating synthetic data assumed to have the same distribution with real data[18] to train machine learning algorithms, these efforts essentially operated as an imputation tool of longitudinal data, but due to unstable training and unsupervised learning, these models were hard to train to generate complex outputs.[19] Missing data remains an issue for evaluation of disease progression.[20,21] Another limitation of existing models is that they focused on the disease deteriorating *per se* rather than on the progressive hazard of an individual patient being converted to AD dementia, such that the censored data could not be statistically accounted for, and inevitably the discovered patterns neglected the individualized temporal difference of conversion to AD dementia.[22,23] Considering that trajectories are heterogenous with varied disease progression rates, it is necessary to incorporate the conversion time into model learning, identify underlying patterns in AD trajectory, and explore their putative causal roles in disease progression to lead to a better understanding of the disease development.

In this study, we aim to address the challenge of identifying underlying patterns in the trajectory of Alzheimer's disease (AD). We view this as a survival

analysis problem and propose a novel deep learning model to tackle it effectively. Unlike traditional approaches that rely on longitudinal data, which can be sparse and irregular in practical settings, we have integrated a deep survival clustering module into our model, allowing us to predictively analyze the progression of AD. The key advantage of our model is the capability to detect the temporal differences in disease progression between individuals. This enables the model to cluster patients into distinct subgroups with unique neuroimaging features as well as varying rates of disease progression. This approach is justifiable because the deep learning model retains temporal information in the representations of patient features through the backpropagation learning process. Consequently, patterns with different progression rates can be reliably identified and leveraged in our analysis.

We hypothesized that, by training our model on AD enriched samples, it would not only explicitly identify essential patterns with different progression rates, but also provide predictions on conversion time to AD dementia for individual participants. First, we extensively validated our model using one simulated and two real-world datasets, ADNI and AIBL. We demonstrated that the progression of AD is a heterogeneous process with varied progression rates in both clinical variables and neuroimaging features. Second, we showed the prediction performance of the derived patterns and our model in time-to-conversion prediction. Additionally, we conducted a Mendelian randomization (MR) analysis to clarify the potential causal link between the discovered patterns and time-to-conversion to AD dementia. An overview of our study design is illustrated in Fig. 1.

Methods

Datasets

We collected demographics, cognitive function score, as well as (longitudinal relaxation time) T1-structured magnetic resonance imaging (MRI) scans from a well-known AD cohort—Alzheimer's Disease Neuroimaging Initiative (ADNI)—for model development and evaluation. Patients recruited in this study were from four cohorts of the ADNI database: ADNI 1, 2, GO, and ADNI 3. Details about the ADNI study can be found in previous publications.[24–26] To study the progression rate between subjects and within different stages of a certain subject, we extracted two datasets from the four ADNI cohorts, corresponding to the transition between sequential stages of AD progression: patients labelled as CN at baseline who were converted to MCI (CN→MCI dataset), and patients labelled as MCI at baseline who were converted to AD (MCI→AD dataset). Patients were labeled according to their clinical diagnosis provided by ADNI. The CN→MCI dataset included 587 patients (315 [53.66%] female, mean age 75 years [Interquartile range (IQR): 71–80]). Among them, 119 (20.27%) were converted from CN to MCI and the other 468 (79.73%) were right censored. Regarding the MCI→AD dataset, there were 783 patients (306 [39.08%] female, mean age 75 years [IQR, 70–81]), of which 348 (44.44%) samples were converted from MCI to AD dementia while the others (55.56%) were right censored. Details of the demographics and clinical variables of the two datasets are summarized in Supplementary Table S3.

Data inclusion criterion

Patients from each dataset were eligible for study inclusion if they had at least two T1-weighted volumetric MRI scans. For patients who had conversion from CN to MCI or from MCI to AD dementia, we selected clinical and MRI data at baseline and at the time of transformation. For censored patients, we selected data at baseline and the last observation time. To ensure that informative clinical variables were selected and the correlation between variables could be diluted, we only included clinical variables with a missing rate smaller than 30% in each dataset.

MRI data acquisition and processing

We extracted both 1.5 T or 3 T MRI data for the selected patients from the ADNI dataset. Then the MRI data was preprocessed using FreeSurfer[27] (version 6.0) through a fully automated pipeline. This process mainly include skull stripping, radiofrequency field (B1) error correction, volume data registration, gray and white matter segmentation, Nonlinear registration of the cortical surface, etc. In this study, we labeled and segmented brain regions according to the Destrieux[28] (2009) brain template. Specifically, each selected T1 structural MRI scan was first registered in the brain template and segmented into 74 brain regions. For each brain region, we extracted cortical surface area, gray matter volume, and average cortical thickness as neuroimaging features from both hemispheres.

Model development

We propose a deep learning model for identifying underlying patterns in AD trajectory, namely, Deep-AD (Fig. 2). The pattern for an individual patient is formalized as a latent representation z which can be derived given the baseline clinical and neuroimaging characteristics x of the patient as well as the patient's progression time t. To this end, we concatenated the baseline clinical features and neuroimaging features extracted from the MRI scans, embedded with t through a transformer encoder, to map to z. Here, $z = \{z_1, z_2, \ldots, z_J\}$ was a latent random vector with dimension J (the predefined number of dimensions which is equivalent to the number of clusters K), which specified different clusters of patients. Hereby, we hypothesized that the captured clusters correspond to distinct patterns of AD trajectories. Specifically, z was sampled through the

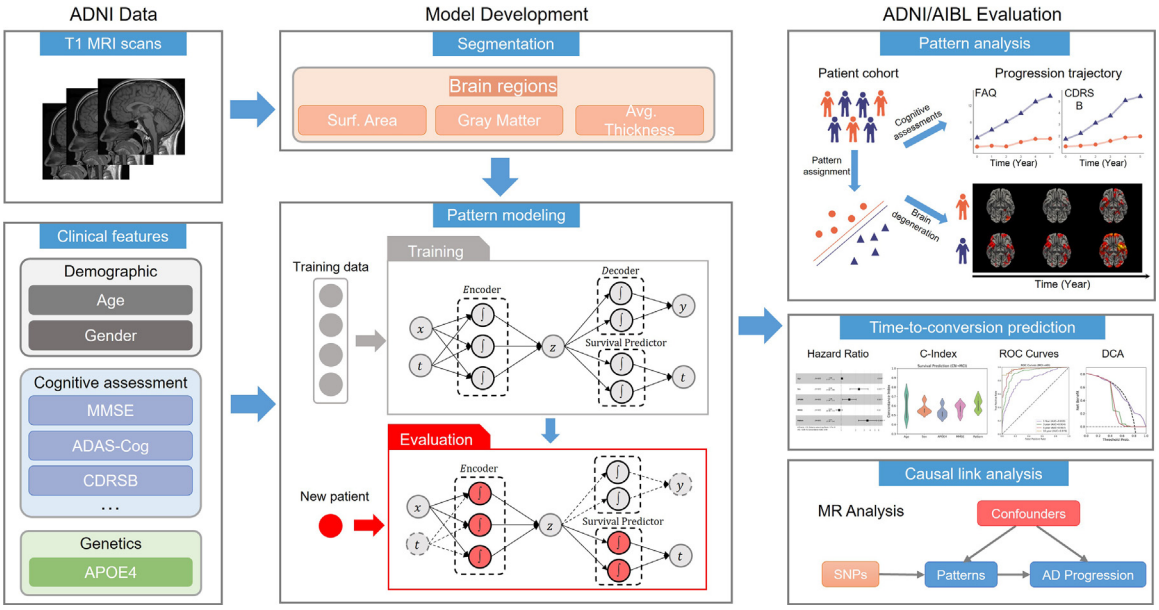

***Fig. 1:* An overview of the study design**. Clinical data, including demographics, cognitive assessments, gene expression, etc., and T1-weighted MRI scans were extracted from the ADNI/AIBL datasets. MRI scans were segmented into discrete brain regions to obtain neuroimaging features: cortical surface area, gray matter volumes and cortical average thickness. Clinical and neuroimaging features were then concatenated and fed into our model to obtain patient representations for clustering. Furthermore, we utilized genome-wide association studies and performed Mendelian randomization analysis to investigate the potential causal links between the discovered patterns and AD progression.

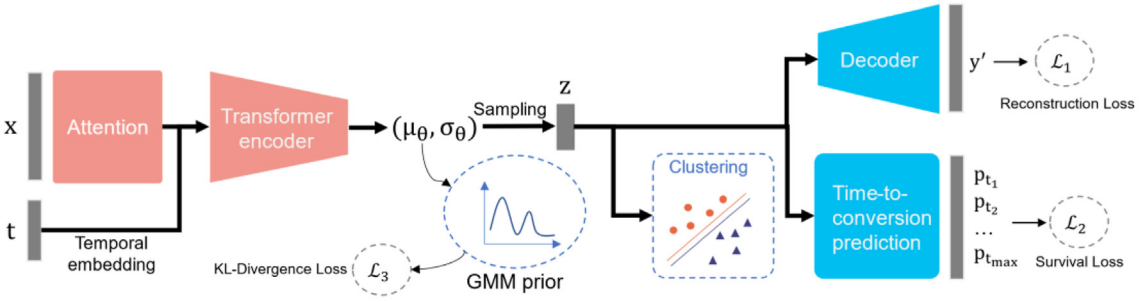

***Fig. 2:* The overall structure for the proposed model: Deep-AD**.

deep variational inference process. We assumed that the prior distribution of z follows a Gaussian mixture distribution,[29] $p(z, k) = \sum_{k=1}^{K} \pi_k \mathcal{N}(\mu_k, \sigma_k)$, where K is the number of clusters, π_k is the prior probability for cluster k, and $\sum_{k=1}^{K} \pi_k = 1$, μ_k, σ_k are mean and standard deviation for the Gaussian distribution of cluster k. Then we used the transformer encoder f_θ to model the mean and standard deviation, $(\mu_\theta, \sigma_\theta)$ of the estimated posterior $q_\theta(z|x, t)$, respectively, thus the reparameterization trick[30] can be used to sample the posterior z by $z = \mu_\theta + \sigma_\theta \cdot \epsilon$.Here ϵ is an auxiliary noise variable sampled from a standard Gaussian distribution $\epsilon \sim N(0, I)$, where I is the identity matrix. By training our model such that the estimated posterior $q(z, k|x, t) = q(z|x, t)q(k|x, t)$ can approximate the prior $p(z, k)$. Thereafter, we estimated the probability that a patient with x and t belongs to cluster k by:

$$q(k|x,t) = p(k|z) = \frac{p(k)p(z|k)}{\sum_{k'=1}^{K} p(k')p(z|k')}$$

Additionally, we learned a transformation function f_γ through a decoder which transforms x to y by the sampled z, which benefits z containing potential information of the disease progression.

We emphasize that we only used the data collected at two time points to train our model, and hereby y is only needed in the training process to build the model. In the inference stage, we only used data x at the starting point

to predictively analyze the disease progression of an individual patient. Furthermore, we hypothesized that patients belong to different patterns have varied progression rates, and used a survival analysis module S_β to estimate the uncensored progression time given the latent representation z for a target patient.

The objective of the proposed Deep-AD is to maximize the likelihood of each unit in the dataset, which mainly consists of three parts: the reconstruction loss for y, log-likelihood loss for survival analysis and the *Kullback-Leibler*-divergence (KLD) of the posterior and the Gaussian Mixture prior. First, the reconstruction loss for y aims at encouraging the model to reconstruct the data well, which can be written as:

$$L(y) = -\mathbb{E}_{q(z,k|x,t)} = -\frac{1}{L}\sum_{k=1}^{K}\sum_{l=1}^{L} p(y|x, z_k)$$

where L is the sample size by Mento Carol (MC) sampling. $p(y|x, z_k)$ is the decoder g that maps x to y by the latent representation z. The decoder g enables the model to learn the progression from x to y. Second, the log-likelihood loss for survival analysis drives the model to learn the distribution of progression time for a target patient, which is defined as:

$$L(t) = \frac{1}{L}\sum_{l=0}^{L}\left[-\mathbb{I}(\delta = 1)\log p_t + \mathbb{I}(\delta = 0)(1 - CIF(t|z))\right]$$

where $\mathbb{I}(\cdot)$ is the indicator function, $\mathbb{I}(true) = 1$, 0 otherwise. $\delta = 1$ indicates that an event occurs (in our case having a progression) for a patient before time t, while $\delta = 0$ indicates censoring. $p(t)$ is the probability of having an event at time t. The first term of $L(t)$ captures the information that a patient has a progression at time t. And the second term follows the knowledge provided by the censored patients who have not yet progressed to the next stage at the censoring time. We use the cumulative incidence function (CIF)[31] to express the cumulative risk of progression for a patient at time t, which is defined as the probability of experience the observed event before t. By this definition, the CIF for an individual patient with the latent representation z and at time t can be estimated as: $CIF(T = \tau|z) = P(T < t|z) = \sum_{t=1}^{\tau} p_t$.

Moreover, the KLD measuring the distance between the estimated posterior $q(z, k|x, t)$ with the prior Gaussian Mixture model $p(z, k)$, regularizes z to the Gaussian Mixture distribution:

$$L(KLD) = D_{KL}\left(q(z, k|x, t)\middle\| p(z, k)\right)$$

Then the full objective can be written as $L = L(y) + L(t) + L(KLD)$. We trained our model for 100 epochs with a batch size of 32 and an initial learning rate of 2×10^{-4}. For optimization, we applied gradient descent to Minimize the total loss L with an Adam optimizer[32] and decreased the learning rate by 20% after every 20 epochs. To better avoid overfitting, we added a dropout layer to each RELU-activated fully connected layer with a ratio of 0.2 and applied weight decay by using L2 regularization to each layer. In terms of number of clusters K, we evaluated our model with K = 2, 3 and 4, respectively. As a result, the 2-cluster model was most preferable, showing the largest temporal difference in the survival curves, whereas the 3- and 4-cluster models did not show significant difference in their progression pathways. Thus, we choose the 2-cluster model as the best fit and interpret the results of the 2-cluster solution. The survival curves for K = 3, 4 and are shown in Supplementary Figs. S2 and S3. More implementation details of the proposed model, including technical and theoretical details of the proposed model and network architecture are presented in Supplementary Method 1.1 and Supplementary Table S2.

For evaluation, we applied five-fold cross validation, and evaluated the differences between the obtained patterns and measured the performance of time-to-conversion predictions by using hazard ratio (HR), concordance index (C-Index), area under receiver operating characteristic curve (AUC), calibration curves, and decision curve analysis (DCA).

Mendelian randomization analysis

Mendelian randomization (MR)[33] is a method that uses the single-nucleotide polymorphisms (SNPs) from genome-wide association study (GWAS) as an instrumental variable (IV) to study the causal effect of an exposure on an outcome. We conducted MR analysis to investigate the causal connection between the identified patterns and AD progression. Before performing MR analysis, we ran GWAS[34] to find potential genetic variants that associate with the discovered patterns. To increase the power of our study, we relaxed the threshold of genome-wide significance ($p < 1.0 \times 10^{-5}$) for instrument selection. We used linkage disequilibrium (LD) clumping ($r^2 > 0.001$) to obtain independent SNPs associated with patterns.[35] Thereafter, we harmonized the exposure and outcome data according to the same effect alleles and removed the palindromic SNPs. Inverse-variance weighted (IVW) method[36] was implemented as the primary method for MR analysis. However, if the genetic variants influence the outcome through a pathway other than through the identified patterns (horizontal pleiotropy), the estimation from the IVW method can be biased.[37,38] To remedy this problem, MR-Egger regression[39] was performed as sensitive analysis to identify the presence of horizontal pleiotropy, where an intercept close to 0 indicated no significant horizontal pleiotropy for the selected SNPs.

Statistical analysis

The proposed Deep-AD is implemented using the python packages "PyTorch" (version 1.8.2) and Scikit-learn (version 1.0.1). We summarized demographical and clinical variables for the experimental cohorts using mean and IQR (interquartile range) for continuous variables, and the frequency of each category of categorical variables. We compared groups stratified by different patterns using student *t*-test for continuous variables and chi-square test for categorical variables. *p*-values of less than 0.050 indicates statistical significance. All statistical analyses were done using R (version 4.2.1). We adopted multivariate imputation by chained equation (MICE) to impute the missing data using R package "MICE" (version 3.14). Random forest is implemented as the main method for imputation. The imputation is performed 5 times, with 5 iterations for each imputation, then the average of the 5 times of imputation is taken as the final imputation result. GWAS on the subtypes was implemented by using the Plink software (version 1.9). The Mendelian randomization analysis was performed using R-package "TwoSampleMR" (version 0.5.6).

External model validation

External validation of the proposed model was performed by using the data extracted from the Australian Imaging Biomarkers and Lifestyle Study of Ageing (AIBL) cohort. In total, there were 203 CN patients (108 [53.20%] female, mean age 73 years [IQR, 68–78], 23 [11.33%] converted to MCI, 180 [88.67%] right censored) and 30 MCI patients (12 [40.0%] female, mean age 77 years [IQR, 71–83], 12 [40.0%] converted to AD dementia, 18 [60.0%] right censored) extracted from the AIBL cohort as the external validation datasets. The data preprocessing procedure was the same as that of ADNI. In comparison with ADNI, several essential covariates (including APOE4, ADAS-cog, etc.) were not available in the AIBL cohort. To remedy it, we assumed that samples in ADNI and AIBL followed the identically independent data distribution, merged data of ADNI and AIBL, and then imputed the missing data of AIBL by using multiple regression algorithm. After that, we assigned participants in AIBL to the patterns learned from ADNI data, and used the model learned from ADNI data to predict the conversion time of AIBL patients.

Ethics

The use of clinical information, and data collection protocols were approved by the ethical committee of College of Biomedical Engineering and Instrument Science, Zhejiang University (number: Zheda Shengyi 2022–3). The study protocol for ADNI was approved by local ethical committees of all participating institutions and all participants signed informed consent.

Role of the funding source

We declare that the funder has no role in study design, data collection, data analysis, data interpretation, writing of the report, and decision to submit the paper for publication.

Results

Validation in a synthetic dataset

We conducted extensive experiments on a synthetic dataset (Supplementary Method 1.2) to verify the capability of our model to (1) capture distinct patterns in AD trajectory, and (2) provide accurate predictions on conversion times to MCI/AD dementia. Specifically, we designed a mapping function to simulate brain atrophy with varied deterioration rates on 40 synthetic MRI regions of interest (ROIs) (Supplementary Method 1.2). Our model not only identified simulated patterns with varied atrophy rates (Supplementary Table S1), but also achieved superior performance than other state-of-the-art models on time-to-conversion prediction in AD trajectory.

Validation in the ADNI cohort

CN→MCI: Deep-AD clustered patients into two independent subgroups (a.k.a. patterns) corresponding to distinct progression patterns: specifically, 403 patients were automatically assigned into the subgroup of pattern 1, of whom 59 [14.64%] patients converted from CN to MCI and 344 were censored; 184 patients were assigned into the subgroup of pattern 2, of whom 60 [32.61%] patients converted from CN to MCI and 124 were censored. **MCI→AD dementia**: Deep-AD clustered patients into two subgroups with distinct progression patterns for MCI→AD: 328 patients were automatically assigned into the subgroup of pattern 1, of whom 53 [16.16%] patients converted from MCI to AD and 275 were censored; 455 patients were assigned into the subgroup of pattern 2, of whom 295 [64.84%] patients converted from MCI to AD and 160 were censored. Additionally, we validated whether field strength, and other factors such as manufacturers would introduce any bias into the results. We treated these factors as fixed effects within the model. Remarkably, our findings remained highly consistent after adjusting for these factors, as demonstrated in Supplementary Fig. S4. This finding indicates the robustness and reliability of our model. Fig. 3 visualizes the discovered patterns on the 2D t-SNE (t-distributed Stochastic Neighbor embeddings). We observed indistinct clusters based on the baseline covariates x in both CN→MCI and MCI→AD datasets (Fig. 3(A) and (B)). By contrast, based on the learned latent representation from the hidden layer of our model, which contains both baseline covariates x and the predicted conversion time information, our model effectively distinguished these two patterns on both datasets.

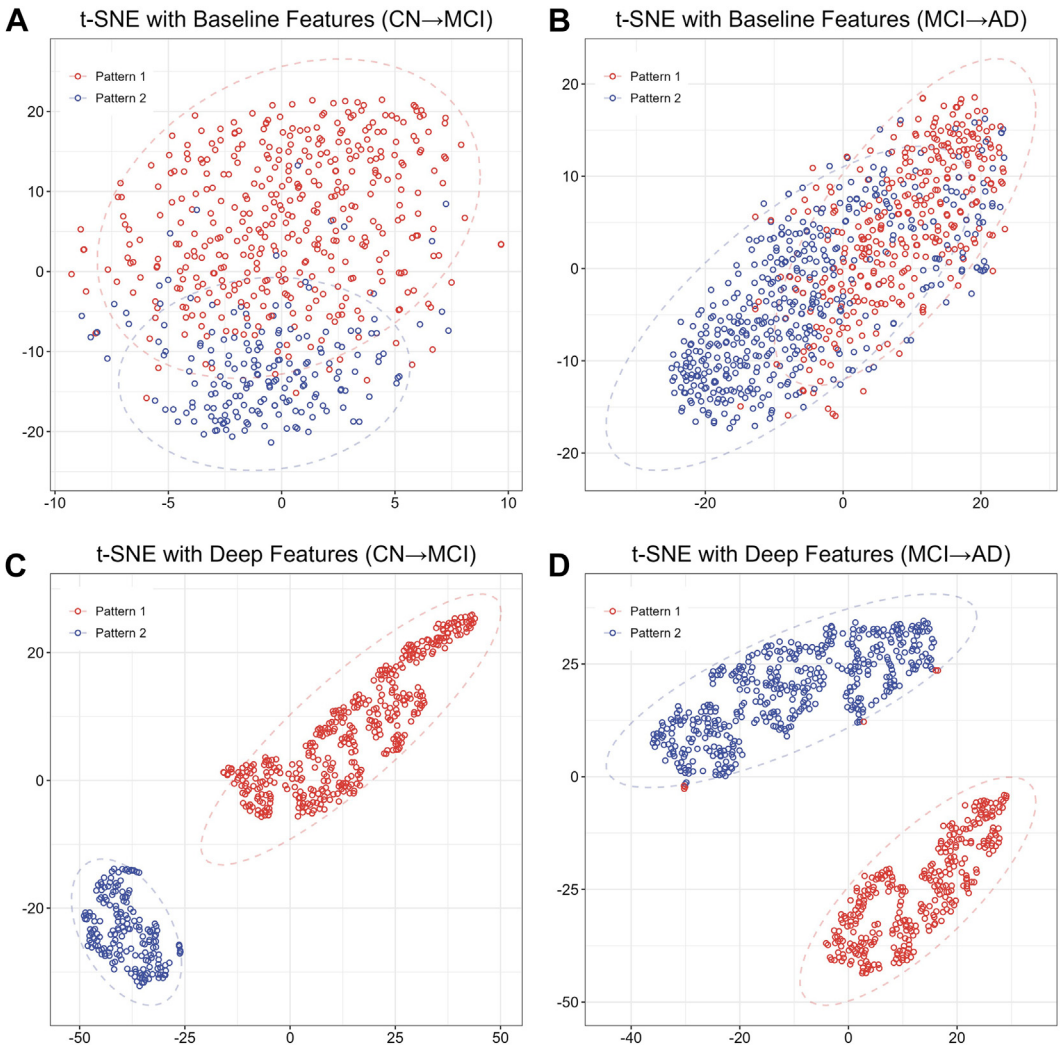

***Fig. 3:* t-SNE for the distribution of the identified patterns on the CN→MCI dataset and MCI→AD dataset.** (A), (B) Two-dimensional (2D) t-distributed stochastic neighbor embeddings (t-SNE) of the baseline features x of the patients with two patterns on the (A) CN→MCI and (B) MCI→AD datasets. (C), (D) 2D t-SNE of by the hidden-layer activations of the model for the two patterns on the (C) CN→MCI and (D) MCI→AD datasets. The hidden-layer features contain the representation of baseline features x and the temporal representation from the conversion time prediction.

The survival curves in Fig. 4 visually indicate the difference in the progression rate of the discovered patterns. Fig. 4(A) illustrates that patients with pattern 2 of CN→MCI exhibited a significantly faster progression rate compared to those with pattern 1 of CN→MCI ($p < 0.0001$). Moreover, Fig. 4(B) reveals that patients with pattern 2 of MCI→AD exhibited a significantly faster progression rate compared to those with pattern 1 of MCI→AD ($p < 0.0001$), and the discrepancy between these two patterns is much larger than that of CN→MCI. Specifically, patients with MCI→AD pattern 2 reached a 50% conversion in less than 30 months, 4 times faster than that of pattern 1 (average of 120 months for conversion).

Evidence has shown that Amyloid β (Abeta) and phosphorylated Tau (pTau) are well-established biomarkers and pathological hallmarks for AD.[40] Survival curves in Fig. 4 demonstrated that patients with positive Abeta (A+) or pTau (T+) status were at higher risk of progression to MCI or AD. Particularly, for patients in the progression of CN to MCI, Abeta/pTau status enriched pattern 1 with significant discrimination power, whereas no significant changes were made by combing pattern 2 with Abeta/pTau status in terms of

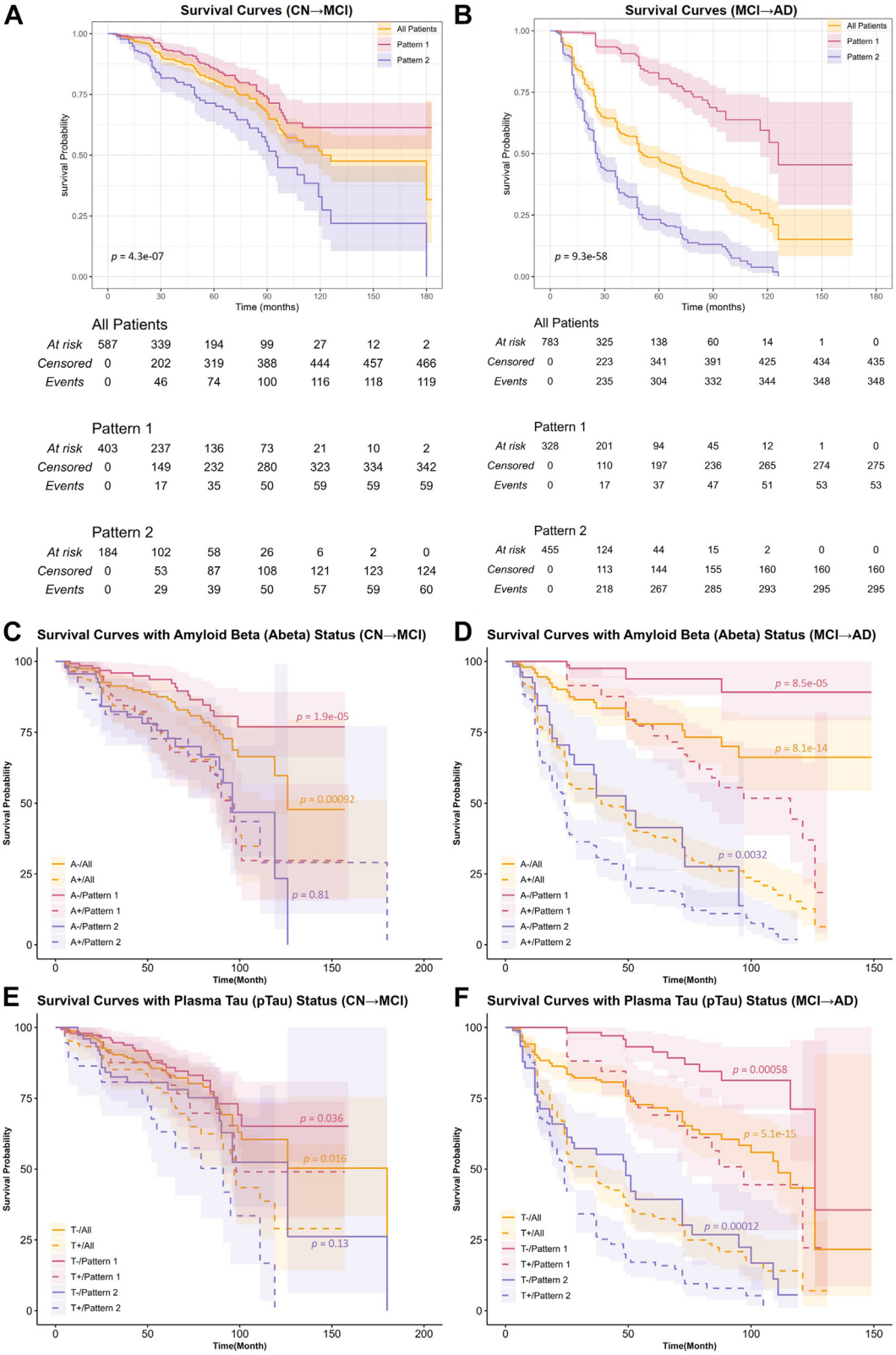
A
Survival Curves (CN→MCI)
All Patients
Pattern 1
Pattern 2
survival Probability
p = 4.3e-07
Time (months)
All Patients
At risk 587 339 194 99 27 12 2
Censored 0 202 319 388 444 457 466
Events 0 46 74 100 116 118 119
Pattern 1
At risk 403 237 136 73 21 10 2
Censored 0 149 232 280 323 334 342
Events 0 17 35 50 59 59 59
Pattern 2
At risk 184 102 58 26 6 2 0
Censored 0 53 87 108 121 123 124
Events 0 29 39 50 57 59 60
B
Survival Curves (MCI→AD)
All Patients
Pattern 1
Pattern 2
survival Probability
p = 9.3e-58
Time (months)
All Patients
At risk 783 325 138 60 14 1 0
Censored 0 223 341 391 425 434 435
Events 0 235 304 332 344 348 348
Pattern 1
At risk 328 201 94 45 12 1 0
Censored 0 110 197 236 265 274 275
Events 0 17 37 47 51 53 53
Pattern 2
At risk 455 124 44 15 2 0 0
Censored 0 113 144 155 160 160 160
Events 0 218 267 285 293 295 295
C
Survival Curves with Amyloid Beta (Abeta) Status (CN→MCI)
p = 1.9e-05
p = 0.00092
p = 0.81
A-/All
A+/All
A-/Pattern 1
A+/Pattern 1
A-/Pattern 2
A+/Pattern 2
Survival Probability
Time(Month)
D
Survival Curves with Amyloid Beta (Abeta) Status (MCI→AD)
p = 8.5e-05
p = 8.1e-14
p = 0.0032
A-/All
A+/All
A-/Pattern 1
A+/Pattern 1
A-/Pattern 2
A+/Pattern 2
Survival Probability
Time(Month)
E
Survival Curves with Plasma Tau (pTau) Status (CN→MCI)
p = 0.036
p = 0.016
p = 0.13
T-/All
T+/All
T-/Pattern 1
T+/Pattern 1
T-/Pattern 2
T+/Pattern 2
Survival Probability
Time(Month)
F
Survival Curves with Plasma Tau (pTau) Status (MCI→AD)
p = 0.00058
p = 5.1e-15
p = 0.00012
T-/All
T+/All
T-/Pattern 1
T+/Pattern 1
T-/Pattern 2
T+/Pattern 2
Survival Probability
Time(Month)

CN→MCI (Fig. 4(C) and (E)). In addition, we observed that Abeta and pTau status added value in differentiating the risk of progression from MCI to AD dementia for patients with both patterns (Fig. 4(D) and (F)), and positive Abeta (A+) or pTau (T+) status significantly increased the risk of conversion to AD dementia.

Table 1 shows several essential clinical covariates and neuroimaging features associated with the identified patterns. In both CN→MCI and MCI→AD dementia cases, patients with pattern 2 (the cluster with higher progression rate), were associated with a larger female population (41.69% vs 79.89% and 24.70% vs 49.45%), lower brain volumes (e.g., hippocampus, entorhinal cortex, and middle temporal gyrus, etc.), and poorer cognitive assessment scores (MMSE, ADAS-cog, etc.). In addition, Apolipoprotein E4 (APOE4), as a significant risk factor for developing AD, was found significantly expressed in the group of patients with pattern 2 of MCI→AD ($p < 0.0001$). However, this difference was not observed in the CN→MCI ($p = 0.89$) cohort (Table 2).

Pattern interpretation

We interpreted the discovered patterns by identifying the most influential clinical covariates and neuroimaging signatures in determining the pattern assignment for an individual patient at baseline. To this end, we measured the shapely value of each covariate, as an indicator of its importance in pattern assignment. Fig. 5(A and B) presents Shapley values of the ten most important predictors, mainly including volumes of brain regions, cognitive and functional assessments, age, and sex. Additionally, we present five commonly used cognitive measurements together with their pattern-wise temporal changes (Fig. 5(C and D)). By analyzing the cluster-wise distribution, we noticed that pattern 2 of CN→MCI/MCI→AD was characterized by faster deteriorating cognitive functions (e.g., CDRSB - Clinical Dementia Rating Scale Sum of Boxes, FAQ–Functional Assessment Questionnaire). Differences in the progression of the two patterns of CN-MCI were relatively mild, especially in the first three years, indicating the challenge of only using cognitive assessments for early prognosis for CN-MCI. In contrast, the progression rates in the two patterns of MCI-AD were dramatically different along the timeline. However, for both CN→MCI/MCI→AD, the two patterns were similar if only considering the baseline cognitive scores, indicating the necessity to take other important features and temporal progression information into account.[41] Supplementary Figs. S10–S13 show the detailed interpretation with all covariates.

Fig. 6 shows that patients with distinct patterns of MCI→AD had distinguished atrophy signatures and progression rates at different time points. From Fig. 6, we observed that patients with pattern 2 of MCI→AD had much faster atrophy rates than those with pattern 1. After one year of progression (Fig. 6(A)), patients with pattern 1 had few signs of atrophy compared to their baselines. On the contrary, patients with pattern 2 had significant atrophy in parts of the frontal and temporal lobes. When progressed to three years (Fig. 6(B)), patients with pattern 1 had slight atrophy in the left temporal pole, left hippocampus and middle frontal gyrus. In contrast, patients with pattern 2 progressed to left fusiform, orbitofrontal cortex and middle temporal gyrus involvement and extended to more frontal and temporal lobes. After five years of progression (Fig. 6(C)), patients with pattern 1 had more atrophy in the cuneus and temporal pole regions. Regarding patients with pattern 2, the atrophic regions gradually progressed from the middle temporal gyrus and the temporal pole to the whole brain. Furthermore, the atrophic regions of patients with pattern 1 were mainly concentrated in cuneus and postcentral gyrus. In contrast, patients with pattern 2 exhibited more atrophy in the regions of medial orbitofrontal cortex, amygdala, and lateral geniculate body.

Time-to-conversion prediction

We used Cox proportion hazard model (CPH)[42] to evaluate the prediction performance of the discovered patterns compared with other clinical covariates. Fig. 7(A) illustrates a significant effect on different patterns in the risk of progression. Specifically, we found that patients with pattern 2 of CN→MCI had a 3.51 ($HR = 3.51$, $p < 0.0001$) times greater risk of progressing from CN to MCI than those with CN→MCI pattern 1. Similar findings were observed on the MCI→AD cohort ($HR = 8.11$, $p < 0.0001$).

Additionally, we evaluated the time-to-conversion prediction performance of using the identified pattern as independent variable, in comparison with clinical well-recognized risk factors of AD (including MMSE, APOE4, etc.).[43] For the identified pattern and each

***Fig. 4:* Survival curves in AD trajectory**. (A), (B). Survival curves for the (A) CN→MCI and (B) MCI→AD datasets. (C), (D) Survival curves stratified by both patterns and Abeta status (A+/A-) on the (C) CN→MCI dataset and (D) MCI→AD datasets. (E), (F) Survival curves stratified by both patterns and pTau status (T+/T-) on the (E) CN→MCI dataset and (F) MCI→AD datasets. Survival curves are estimated using Kaplan–Meier's (KM) method and stratified by different patterns. The p-value derived by log-rank test indicates a statistically significant difference between the two patterns on each dataset. Survival tables below the survival curves show the number of patients currently at risk, censored, or having an event (event representing progression from CN to MCI or from MCI to AD dementia) at each time point corresponding to the x-axis.

Features	Pattern 1 (N = 403)	Pattern 2 (N = 184)	p-value
Sex			<0.0001
Female	168 (41.69%)	147 (79.89%)	
Male	235 (58.31%)	37 (20.11%)	
No. MCI	59 (14.64%)	60 (32.61%)	**<0.0001**
progression/censoring time (month)	51.99 (25.00–75.00)	48.64 (24.75–72.00)	0.29
Age at baseline	74.81 (69.93–79.07)	76.91 (72.18–81.60)	**<0.0001**
APOE4			0.89
0	278 (69.98%)	125 (67.93%)	
1	114 (28.28%)	55 (29.89%)	
2	11 (2.73%)	4 (2.17%)	
CDRSB	0.15 (0.00–0.00)	0.26 (0.00–0.50)	**0.0025**
ADAS11	5.77 (3.33–8.00)	6.39 (4.33–8.00)	**0.0014**
MMSE	28.96 (28.00–30.00)	28.68 (28.00–30.00)	**0.0019**
Ventricles (mm^3)	36,777.11 (21,977.10–46306.03)	34,552.27 (20,778.70–43928.00)	0.0058
Hippocampus (mm^3)	7527.89 (6986.50–8104.20)	6793.69 (6221.75–7379.45)	**<0.0001**
WholeBrain (mm^3)	1,066,547.96 (1,004,525.00–1121,875.00)	940,013.73 (895,673.25–982,180.50)	**<0.0001**
Entorhinal (mm^3)	4069.55 (3626.00–4461.50)	3569.15 (3140.75–4043.50)	**<0.0001**
Fusiform (mm^3)	18,610.71 (17,187.50–20117.00)	16,539.32 (15,158.50–17802.50)	**<0.0001**
MidTemp (mm^3)	21,195.97 (19,434.25–22698.50)	18,263.00 (16,888.50–19635.00)	**<0.0001**
ICV (mm^3)	1,539,166.12 (1,448,545.00–1634,107.50)	1,383,899.33 (1,295,902.50–1454,727.50)	**<0.0001**

Abbreviations: No. MCI/AD, Number of patients converted to MCI/AD; APOE4- Number of Apolipoprotein E4 alleles; CDRSB, Clinical Dementia Rating Scale Sum of Boxes (boxes are the six domains for evaluating dementia); ADAS-cog, Alzheimer's Disease Assessment Scale–Cognitive Subscale; MMSE, Mini–Mental State Examination; MidTemp, Middle Temporal Gyrus; ICV: Intracerebral Volume. p-value was calculated by the chi-square test for discrete and t-test for continuous variables. Mean and variance were provided for numerical variables. $p < 0.05$ are indicated in bold.

Table 1: **Statistical comparisons of clinical and neuroimaging features of the discovered patterns on the (A) CN→MCI.**

features	Pattern 1 (N = 328)	Pattern 2 (N = 455)	p-value
Sex			**<0.0001**
Female	81 (24.70%)	225 (49.45%)	
Male	247 (75.30%)	230 (50.55%)	
No. AD	53 (16.16%)	295 (64.84%)	**<0.0001**
progression/censoring time (month)	48.28 (25.00–64.25)	27.19 (12.50–36.00)	**<0.0001**
Age at baseline	74.19 (69.20–79.40)	75.59 (70.60–81.10)	**0.00030**
APOE4			**<0.0001**
0	191 (58.23%)	181 (39.78%)	
1	108 (32.92%)	205 (45.05%)	
2	29 (8.84%)	69 (15.16%)	
CDRSB	1.58 (0.50–2.00)	2.70 (1.50–3.88)	**<0.0001**
ADAS11	9.64 (6.00–12.00)	14.11 (10.00–17.59)	**<0.0001**
MMSE	27.54 (26.00–29.00)	25.76 (24.00–28.00)	**<0.0001**
Ventricles (mm^3)	44,424.04 (27,762.25–56771.32)	46,684.13 (30,217.50–59022.32)	0.059
Hippocampus (mm^3)	7077.91 (6402.98–7744.00)	6008.17 (5340.10–6677.00)	**<0.0001**
WholeBrain (mm^3)	1,077,291.53 (1,018,032.50–1137,240.00)	971,404.66 (904,813.25–1030,115.00)	**<0.0001**
Entorhinal (mm^3)	3790.83 (3310.00–4255.00)	3075.93 (2571.75–3577.25)	**<0.0001**
Fusiform (mm^3)	18,556.20 (17,052.75–20277.00)	15,927.66 (14,245.00–17523.75)	**<0.0001**
MidTemp (mm^3)	20,812.21 (18,969.00–22601.00)	17,771.77 (16,017.25–19364.50)	**<0.0001**
ICV (mm^3)	1,587,973.84 (1,497,325.00–1686,807.50)	1,507,146.51 (1,382,177.50–1604,485.00)	**<0.0001**

Abbreviations: No. MCI/AD, Number of patients converted to MCI/AD; APOE4- Number of Apolipoprotein E4 alleles; CDRSB, Clinical Dementia Rating Scale Sum of Boxes (boxes are the six domains for evaluating dementia); ADAS-cog, Alzheimer's Disease Assessment Scale–Cognitive Subscale; MMSE, Mini–Mental State Examination; MidTemp, Middle Temporal Gyrus; ICV: Intracerebral Volume. p-value was calculated by the chi-square test for discrete and t-test for continuous variables. Mean and variance were provided for numerical variables. $p < 0.05$ are indicated in bold.

Table 2: **Statistical comparisons of clinical and neuroimaging features of the discovered patterns on the (B) MCI→AD dataset.**

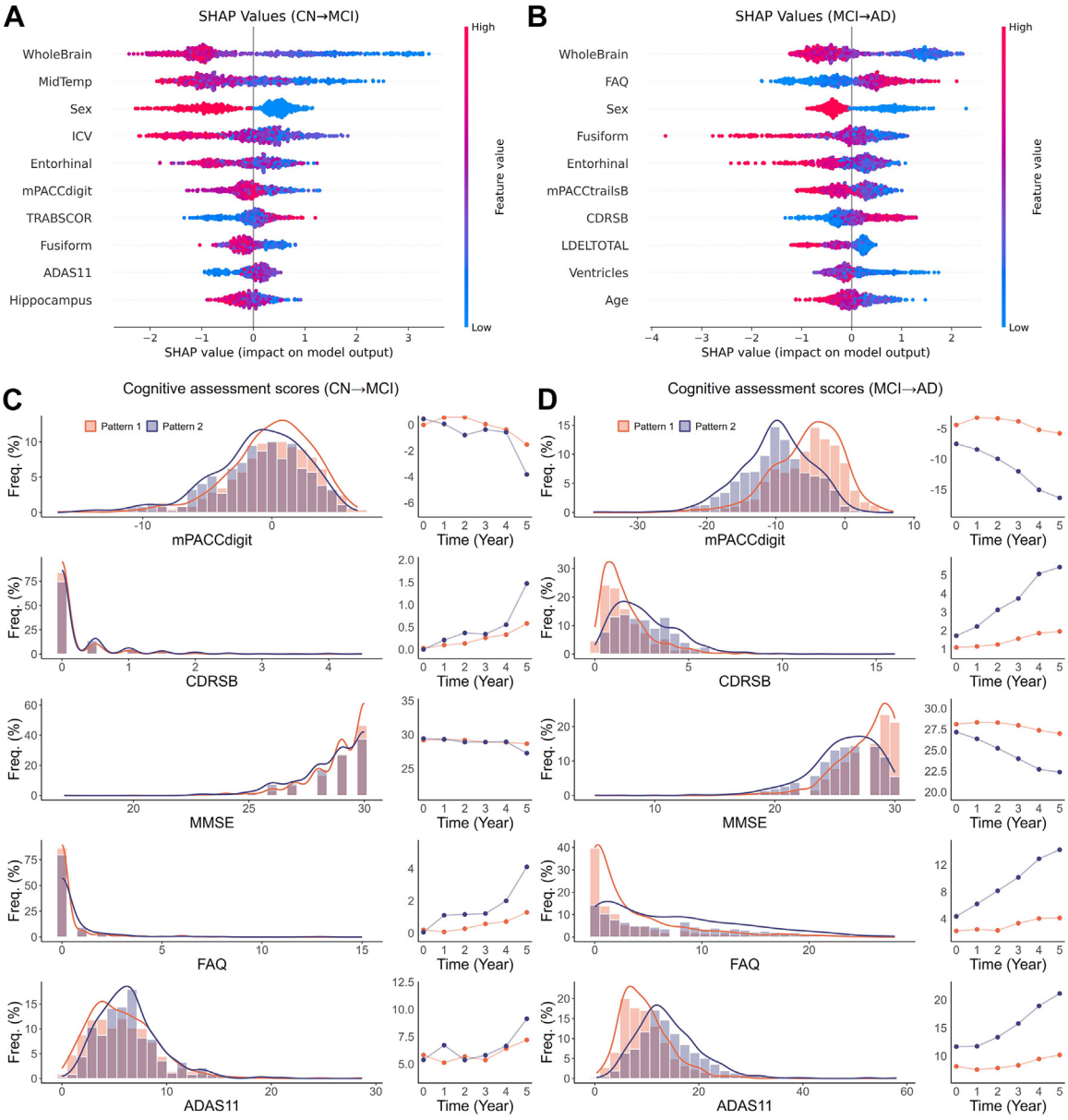

Fig. 5: **The most important predictors for disease progression pattern assignments**. (A), (B) Beeswarm plots of the ten most important predictors on the (A) CN→MCI and (B) MCI→AD datasets, respectively. The SHAP value of a predictor reflects its contribution to distinguish the two patterns (a SHAP value > 0 indicates more pattern 2, and <0 more pattern 1). The color scale shows the value of the feature, where red indicating a larger value and blue indicating a smaller value. (C), (D) The pattern-wise distribution of 5 cognitive assessment scores and their changes over time on the (C) CN→MCI and (D) MCI→AD datasets, respectively. All available patients with 5 years of follow-up were selected to show how these cognitive assessment scores change over time. Abbreviations: MidTemp: middle temporal gyrus, ICV: intracerebral volume, mPACCtrailsB: Preclinical Alzheimer's Cognitive Composite Trails B, LDELTOTAL: logical memory delayed recall total, mPACCdigit: Preclinical Alzheimer's Cognitive Composite Scores, CDRSB: Clinical Dementia Rating Scale Sum of Boxes, MMSE: Mini-Mental State examination, FAQ: Functional Activities Questionnaire, ADAS11: Alzheimer's Disease Assessment Scale-Cognitive Subscale (11 items).

baseline variable, we constructed a single-variable CPH model and reported the concordance index (C-Index) results by 5-fold cross-validation. As can be seen in Fig. 7(B), the discovered patterns outperformed all the selected variables and were able to achieve an average cross-validated C-Index of 0.618 (95% CI 0.602–0.634) for prediction of the progression from CN to MCI. Similarly, we achieved an average C-Index of 0.718 (95% CI 0.712–0.725) for predicting the conversion time from MCI to AD dementia.

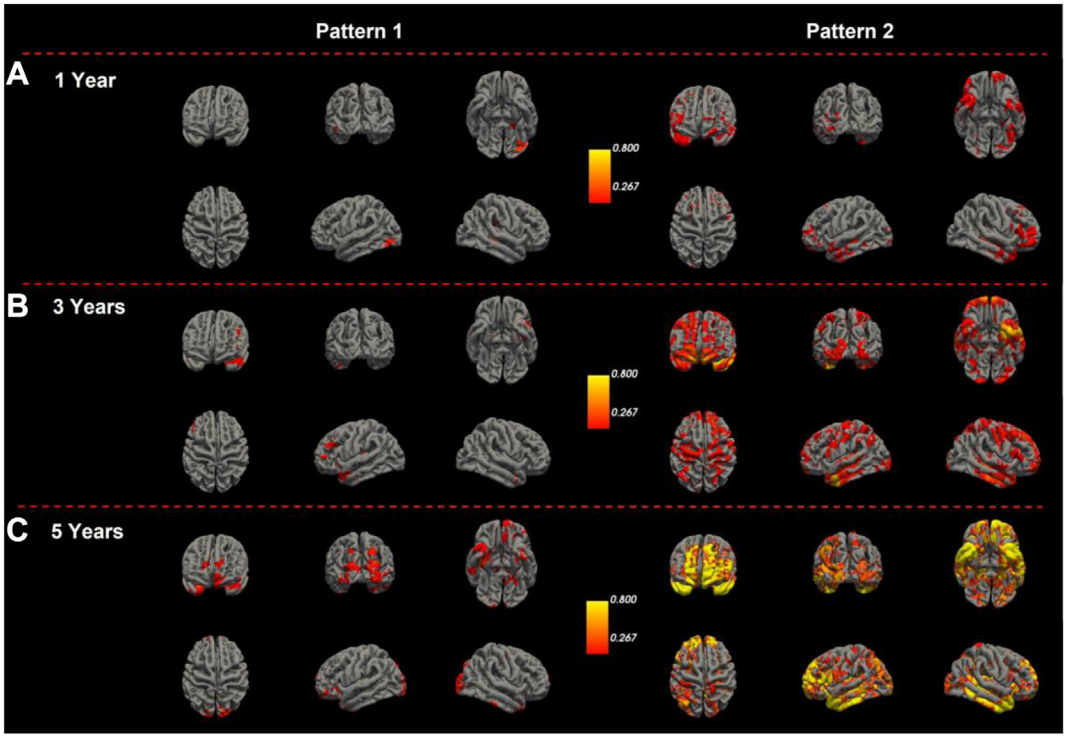

Fig. 6: **Atrophy of the identified patterns at different time points**. MRI scans of available patients (including subsequently censored ones) at the three time points, i.e., (A) 1-, (B) 3-, and (C) 5-year, were collected to compare the difference of brain atrophy between the discovered patterns (left: Pattern 1, right: Pattern 2). The diagrams show the difference of atrophies of brain regions at each time point compared to the baseline. The color scale illustrated the fraction of patients with atrophy in a certain brain region (red color: less atrophy, yellow color: more atrophy).

As illustrated in the ROC curves evaluated at 1, 3, 5 and 10 years (Fig. 7(C)), our model achieved consistently impressive performance on predicting the progression time of AD dementia/MCI onset with an AUC of 0.708–0.886 and 0.810–0.979 on the CN→MCI and MCI→AD cohorts, respectively. It is worth noting that our model is largely superior to the survival analysis models using MMSE (0.537–0.600) or APOE4 (0.564–0.681) as predictors (ROC results for using MMSE and APOE4 are shown in the Supplementary Fig. S6). In addition, as shown by the DCA curves in Fig. 6 (D), the proposed Deep-AD provided significantly larger net benefits across the range of the threshold progression risks than the survival analysis models using MMSE or APOE4. Moreover, the performance of our model is substantiated by the results from C-Index, ROC curves, Calibration curves, and DCA (Supplementary Tables S6–S8 and Supplementary Figs. S7–S9), consistently highlighting the exceptional predictive capability of our model when compared to the conventional and state-of-the-art machine learning models.

External validation in the AIBL cohort

We externally validated our model in a cohort of participants from the AIBL database (203 CN→MCI; 30 MCI→AD) (details of the demographics and clinical variables of the AIBL datasets are summarized in Supplementary Table S4). The conversion rates were 11.3% (N = 23) and 40.0% (N = 12) for CN→MCI and MCI→AD, respectively, indicating that most of CN patients were censored while over half of MCI patients were transformed into AD dementia. Compared with the ANDI cohort, more participants in the AIBL CN→MCI dataset were cognitive normal; they were also generally younger and had higher values of MMSE. Supplementary Fig. S15 shows that the proposed model clustered AIBL participants into distinct patterns with statistically different survival curves.

Regarding the conversion time prediction, the proposed Deep-AD demonstrated competitive prediction performance (C-Index: CN→MCI 0.693 [95% CI, 0.667–0.717]; MCI→AD 0.752 [95% CI, 0.698–0.807]), in comparison with clinical widely used risk factors of AD, i.e., age (C-Index: CN→MCI 0.516 [95% CI, 0.474–0.558]; MCI→AD 0.409 [95% CI, 0.337–0.482]), sex (C-Index: CN→MCI 0.581 [95% CI, 0.552–0.611]; MCI→AD 0.545 [95% CI, 0.513–0.578]) and MMSE (C-Index: CN→MCI 0.672 [95% CI, 0.632–712]; MCI→AD 0.730 [95% CI, 0.682–0.778]) (Supplementary Fig. S15(B)) (Different from ADNI, APOE4 was not

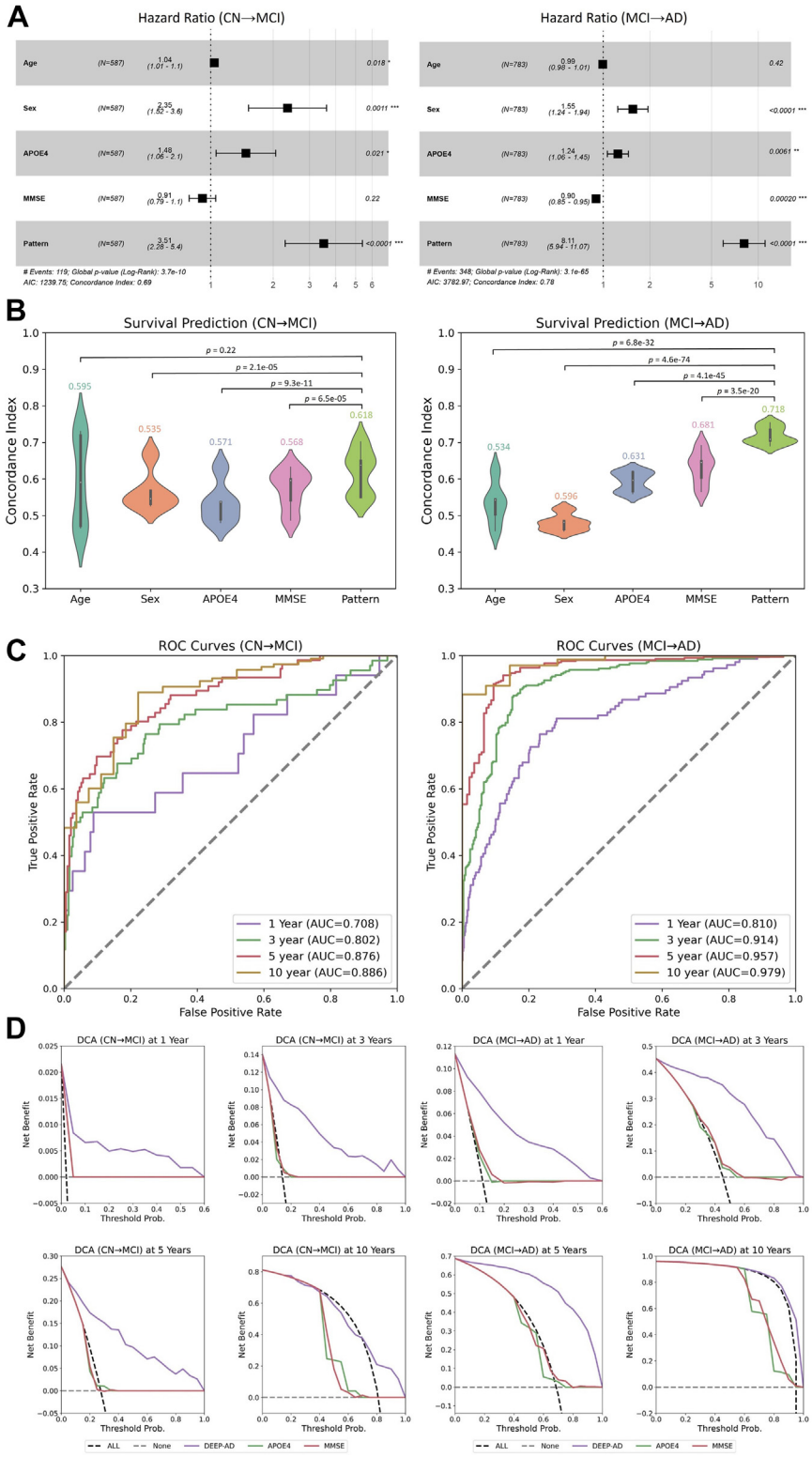

***Fig. 7*: Evaluations of time-to-conversion prediction**. (A) Time-to-conversion predictions comparison of Hazard ratio (HR) for derived patterns with other clinical features on the CN→MCI and MCI→AD datasets. HR estimates how the risk of progression for each unit increase of a particular variable. An HR of 1 means no modification of the risk, HR > 1 means there is an increase in the risk, and an HR < 1 means there is a

available in the AIBL cohort). A similar pattern of results in terms of AUC and DCA was observed on 3- and 5-year predictions, with consistently comparative performance with MMSE (Supplementary Fig. S15(D)).

Causal link estimation

We conducted GWAS on the discovered patterns as phenotypic outcome, i.e., pattern 2 as outcome and pattern 1 as normal control. Genetic variants were available on 252 subjects (163 pattern 1, 89 pattern 2) in the CN→MCI cohort, and on 380 subjects (183 pattern 1, 197 pattern 2) in the MCI→AD cohort. As can be seen in Fig. 8, no genetic variant was found higher than the predetermined threshold 5.0×10^{-8}. Due to the small sample size for the GWAS analysis, a high threshold may easily lead to false negatives. To alleviate it, we lowered the significant threshold for the p-value to 1.0×10^{-5} [44], and observed that four SNPs (rs6679625 at chr1 [p = 3.5e-06], rs7540920 at chr1 [p = 8.1e-06], rs4839882 at chr6 in KLHL32 [p = 2.4e-06] and rs10898826 at chr11 in ANO1 [p = 9.77e-06]) were statistically significantly associated with patterns in the progression of CN to MCI, and three SNPs at chr18 in DSEL-AS1 (rs176004 [p = 6.1e-06], rs393881 [p = 6.1e-06], rs281552 [p = 8.2e-06]) were associated with patterns in the progression of MCI to AD dementia. Summary information of SNPs found by GWAS is presented in Supplementary Table S9.

To investigate the causal relationships between the identified patterns and AD, we conducted MR analysis to examine if there is a causal effect between patterns and two potential outcomes, i.e., AD onset and the conversion time to AD dementia. While Table 3 shows that no significant causal effect was detected between the identified patterns and AD onset, a suggestive causal association between the identified patterns of MCI→AD and the conversion to AD dementia in 1- and 3-years was observed (IVW p = 0.00010 for one-year progression and p = 2.8e-07 for three years progression) (Table 4). The MR-Egger intercepts of the 1- and 3-years of progression were close to zero and the p-value >0.050, indicating no evidence of horizontal pleiotropy were detected. Additionally, we found that the identified patterns showed a positive effect (Beta >0) with the 1- and 3-years progression of MCI to AD, indicating that patients with MCI→AD pattern 2 were causally associated with a higher risk of progression within 1- or 3-years than those patients with pattern 1.

Discussion

In this study, we developed, validated, and evaluated a novel deep learning model for identifying underlying patterns in AD trajectory. By capitalizing on the rich real-world data from the ADNI and AIBL cohorts and a deep survival clustering technique, we were able to overcome the challenges associated with lacking longitudinal data and deficiency in individualized time-to-conversion prediction. Note that our model learned nonlinear transformation from real-world complex data rather than generated/concatenated data, thereby provided a realistic representation of clinical biomarkers and neuroimaging signatures for an individual patient. We emphasize that, instead of modeling the disease progression on the longitudinal data, we only used the data collected at two time points to train our model, and the data at baseline (i.e., starting time point) for inference to predictively analyze the trajectory of an individual patient. This learning strategy alleviates the problem of lacking longitudinal data.

The findings on real-world ADNI and AIBL data highlighted the value of our model to effectively identify biologically and clinically distinct patterns in AD trajectory. Extensive experimental results demonstrated that there existed robust differences between the identified patterns in biomarker compositions, cognitive scores, brain regional atrophies, and genetic backgrounds. Model interpretation through SHAP values revealed the crucial role played by whole brain, entorhinal cortex, and fusiform gyrus in distinct patterns of both CN→MCI and MCI→AD progression (Fig. 5(A and B)), indicating these regions emerges as a pivotal neural signature for distinguishing the progression patterns of AD.[45–47] Notably, our analysis also highlighted that the hippocampus is associated with the progression patterns of CN→MCI (Fig. 5(A)), suggesting that it is an essential marker in the initial stage of AD progression.[48] Evidence has shown that hippocampus is vulnerable to deterioration during early-stage Alzheimer's disease (AD), leading to memory and cognitive impairment.[48,49] In addition, our results also confirmed that patients with pattern 2 of MCI→AD progressed more rapidly and were highly associated with females (Fig. 5(A and B)).

reduction of the risk. (B) Predictive ability of the identified patterns on the CN→MCI and MCI→AD datasets. We evaluated the performance of time-to-conversion prediction by C-Index and compared the performance of the discovered patterns of other 4 clinical variables: age, sex, APOE4 and MMSE. The violin plots showed the 5-fold cross-validated C-Index results for each variable. (C) ROC curves for prediction of conversion time on the CN→MCI and MCI→AD datasets. We accessed the ROC curves for 1, 3, 5 and 10 years of progression from CN to MCI and from MCI to AD dementia. (D) Decision Curve Analysis (DCA) for prediction of conversion time on the CN→MCI and MCI→AD datasets. DCA graphically shows the clinical usefulness of a survival analysis model based on a continuum of potential thresholds of conversion risks (x axis) and the net benefits to time-to-conversion prediction (y axis). The two baseline curves in black and gray stand for the assumption that all patients (ALL) and no patient (None) will progress to the next stage, i.e., CN to MCI and MCI to AD dementia.

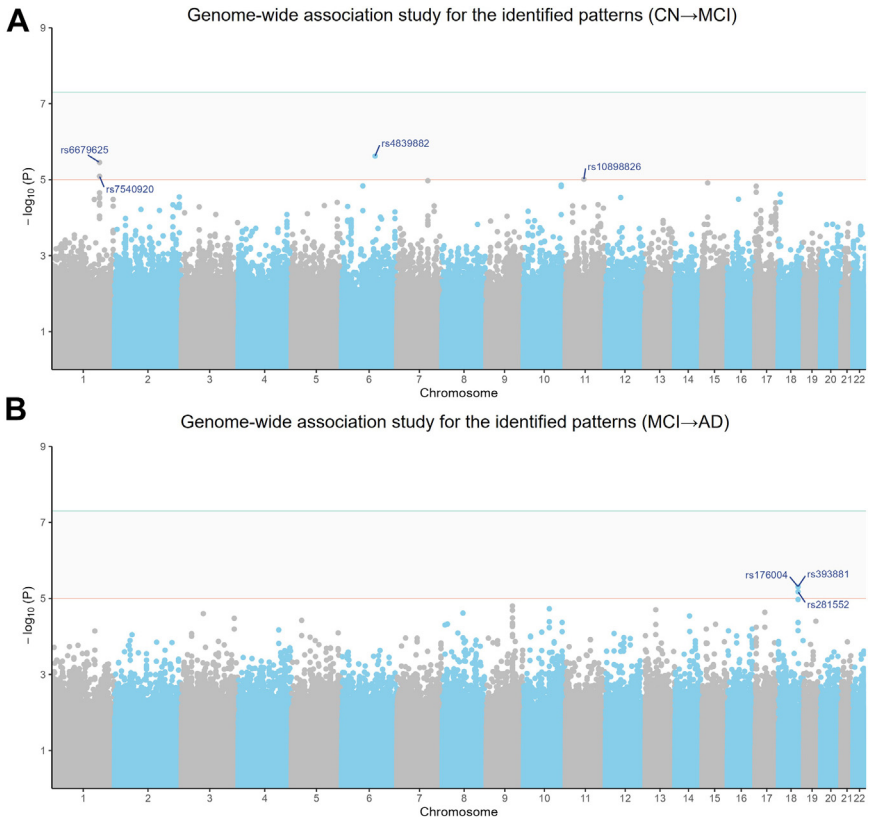

Fig. 8: **Manhattan plots of genome-wide association study (GWAS) on the (A) CN→MCI and (B) MCI→AD datasets**. Manhattan plots show the strength of the association between each SNP and phenotype (pattern) on each chromosome. Each point in the Manhattan plot represents the location of a SNP on the chromosome (x-axis) and the strength of its association (y-axis). The Red lines represent the threshold of *p*-value for genome-wide significance, i.e., $p = 1.0 \times 10^{-5}$.

As pointed out by Payami et al.,[50] women have a higher risk of developing AD compared with men. Furthermore, our results revealed the heterogeneity of brain atrophy in trajectories of AD patients. Intuitively, patients with pattern 1 of MCI→AD had mild atrophy in their occipital lobe and posterior frontal lobe, mainly including cuneus and postcentral gyrus. On the contrary, patients with pattern 2 of MCI→AD were associated with faster degeneration rate in their medial orbitofrontal cortex, amygdala, and lateral geniculate body, implicitly indicating that it is a group of early-onset AD patients with a fast brain atrophy rate across multiple pathologies.[17,18,51] Moreover, a significant difference in the expression of APOE4 was observed in the discovered patterns of MCI→AD, but there was no statistically difference in APOE4 observed in the progression of CN→MCI. We hypothesized that APOE4 allele is rarely expressed in the early stages of AD, such that it is not critical/essential to distinguish the progression rate of CN transformation into MCI. Without doubt, the interpretability of the discovered patterns would make them more amenable to medical practitioners.

It is worth mentioning that our model did not explicitly model disease stages, but preserved the temporal semantics of individual patients along the timeline of their disease development through the time-to-conversion analysis. This is critical since patients may have individual characteristics at enrollment, and varied progression rates due to the heterogenous trajectory of AD.[52] As indicated in Fig. 3(A and B), using baseline patient covariates may cluster out indistinct patterns. In contrast, our model developed a deep survival clustering approach to adjust for patients' baseline time and align

Dataset	Outcome	Method	Beta	SE	*p*-value (IVW)
CN→MCI	AD	IVW	0.012	0.009	0.18
MCI→AD	AD	IVW	−0.005	0.015	0.74

Table 3: **Mendelian randomization tests for the discovered patterns with AD onset.**

	Outcome	Beta	SE	p-value (IVW)	MR-Egger intercept	horizontal pleiotropy (p-value)
CN→MCI	1-year progression	0.211	0.254	0.36	−4.260	0.37
	3-year progression	−0.061	0.206	0.77	−1.995	0.52
	5-years progression	−0.033	0.151	0.82	0.454	0.84
	10-years progression	0.034	0.121	0.78	0.031	0.99
MCI→AD	1-year progression	0.789	0.205	0.00010	0.310	0.99
	3-year progression	0.685	0.133	2.8e-07	0.097	0.99
	5-years progression	0.808	0.126	1.5e-10	1.660	0.92
	10-years progression	0.604	0.122	7.0e-07	1.280	0.93

We used the inverse-variance weighted (IVW) method to access the causal relationship between exposure and outcome, and a p-value <0.050 indicates a significant causal relationship. For sensitive analysis, we used MR-Egger to test the horizontal pleiotropy for the selected SNPs. The MR-Egger intercept was used to assess the horizontal pleiotropy, where an intercept close to zero indicates no horizontal pleiotropy was detected.

Table 4: **Mendelian randomization tests for patterns with the conversion time to AD in 1, 3, 5 and 10 years.**

them on the time axis, such that the latent representations of distinct patterns containing both patient covariates at baseline and the estimated conversion times can be well extracted (Fig. 3(C and D)). In this sense, the identified patterns were inherently linked to disease progression with HR up to 3.51 and 8.11 in CN→MCI and MCI→AD cohorts, respectively, and thus would have better predictive power than the conventional clinical features and cognitive measurements. Particularly, the prognostic model built on the identified pattern performed significantly better than those built on the conventional demographics and clinical biomarkers (e.g., age, sex, MMSE, APOE4, etc.) in predicting an individual patient's time-to-conversion to MCI/AD dementia, in terms of different quantitative evaluation measures, as summarized in Fig. 7 and Supplementary Fig. S15. These findings demonstrate that the identified pattern could act as a surrogate for prognosis, if APOE4 or cognitive measurements is not available.

The growing utilization of the Amyloid Tau Neurodegeneration (ATN) biomarkers[53,54] provides an opportunity for accurate diagnosis and precision therapy for AD patients. Previous findings demonstrated that positive amyloid/tau status is related to cognitive decline and future progression to dementia.[55] Our results substantially confirmed these findings, showing that patients who were amyloid positive (A+) or tau positive (T+) were linked to an increased risk for AD progression (Fig. 4). Specifically, patients with A+ and T+ were significantly represented in pattern 2 of MCI→AD (Supplementary Fig. S5), where 80.36% patients were present with A+ and 67.14% patients with T+. In contrast, only 53.05% and 38.03% patients with pattern 1 of MCI→AD were present with A+ and T+, leading to a slow rate for progression to AD dementia. Moreover, we found that the two patterns exhibited significantly different progression rates for patients with A+/T+ (Fig. 4(C)–(F)). These findings indicate that the identified patterns could offer complementary performance to an AT (N)-based solution for disease progression prediction.

We conducted GWAS and MR analysis to investigate the causal relationship between the identified patterns and the progression rates in AD trajectory. Analysis results suggested that the discovered patterns were causally associated with the varied progression rates of MCI transformation into AD dementia (Table 4). Although an abundance of genetic studies has provided plentiful evidence that late-onset AD has heritability estimates of 58–79%,[56,57] few of existing studies clearly elucidated the genetic backgrounds associated with the rate of deterioration of AD. On the contrary, our study revealed three potential genetic variants at chromosome 18 in DESL-AS1, suggestively associated with the progression of AD. Despite the disclosed genetic variants were not causally associated with the occurrence of AD, as indicated in previous GWAS studies of AD,[58] they were causally associated with the discovered patterns of MCI transformation into AD dementia, indicating that these genetic variants lead to the faster progression speed for patients with pattern 2 of MCI→AD than those with pattern 1. These findings demonstrated that the identified MCI→AD patterns revealed distinct underlying subtypes of neurodegeneration, differing not only in their biomarker composition, cognitive scores and imaging signatures, but also in genetic backgrounds. DSEL-AS1 was previously found to be associated with several psychiatric disorders, such as unipolar depression,[59] and bipolar disorder,[60] indicating that faster progression of AD may share genetic risks with these psychiatric disorders. It deserves further investigations on this potential genetic connection. Moreover, no causal link was found between the identified patterns and the progression rate of CN→MCI. However, it does not necessarily mean that there is no causal link between them. Since the progression from CN transformation into MCI is often modest and hard to track, it may increase the imperceptibility for identifying the changes in their clinical features and worth

further careful investigation. Hence, the causal relationship between the identified patterns and progression rate of CN→MCI may not be well captured. Overall, our findings highlighted the utility of MR analyses to draw on potentially causal links between patterns and the progression rates of AD.

Despite promising findings, some limitations of our study should be addressed. First, we trained and evaluated our model on ADNI data, with an external validation in the AIBL cohort. We argue that the proposed model is generalizable and can be applied to any long-term disease progression analysis. To further increase the generalizability of our model, external validation could be performed on other large datasets to verify whether the discovered patterns are consistent across diverse populations. This is left for future work. Second, we trained our model by using data extracted from two time points to analyze the disease progression in a predictive manner. Although this learning strategy relaxed the problem of longitudinal data restriction, the progression information between the two time points should be appropriately collected and well exploited to analyze the disease development in a fine-grained manner.[61,62] Another limitation is the insufficient sample size for GWAS analysis which may lack statistical power. However, we still find evidence for associations between the identified patterns and the progression of AD in the MR analysis, which may require further validation using a large-scale sample of data. Lastly, only retrospective data was used in this study, highlighting the need for a standardized pipeline for long-term prospective data collection in the future.

In summary, we presented a novel deep learning model to identify underlying patterns in AD trajectory. The obtained experimental results on a range of synthetic and real-world datasets highlighted the effectiveness of our model in identifying biologically and clinically meaningful patterns regulated by different progression rates while remaining competitive at time-to-conversion prediction. External validation also demonstrated the generalization ability and clinical utility of our model, particularly by providing clinicians with a cost-effective manner in stratifying patients about the likelihood of progression to MCI/AD dementia within a specific time period, and therefore potentially facilitating enrollment in clinical trials. Our approach has the potential to serve as a tool for precision medicine and could be applied to any long-term progressive diseases, including but not limited to AD or other neurodegenerative disorders.

Contributors

ZH, YCZ, YYZ and MP conceived and designed the study. FY developed and validated the deep learning system supervised by ZH and FW with clinical input from YCZ, JY, ZYL and FFZ. FY and AH did the statistical analysis. FY, ZH and YYZ also contributed to computational analysis and validations. FW provided critical reading and suggestions. FY, YYZ and ZH drafted the manuscript with input from YCZ, JY, MP and JS. ZH and YCZ contributed equally to the work as senior authors. All authors subsequently critically edited the report. All authors read and approved the final report. The corresponding author and senior authors had full access to all data. All authors had full access to all the data in the study and had final responsibility for the decision to submit for publication.

Data sharing statement

The data that support the findings of this study were obtained from the Alzheimer's Disease Neuroimaging Initiative (ADNI) and Australian Imaging Biomarkers and Lifestyle Study of Ageing (AIBL), which are available from the ADNI database (https://adni.loni.usc.edu) and AIBL database (https://aibl.csiro.au/) upon registration and compliance with the data use agreement. The source codes pertaining to both the proposed deep learning model and data analysis in this manuscript are provided at https://github.com/ZJU-BMI/disease_progression_patterns.

Declaration of interests

All authors declare no competing interests.

Acknowledgements

This work was partially supported by the National Key Research and Development Program of China under Grant No 2022YFF1202400, the Key R&D Program of Zhejiang under Grant No. 2022C03134, and the National Nature Science Foundation of China under Grant No. 82272129. Data used in preparation of this article was obtained from the Alzheimer's Disease Neuroimaging Initiative (ADNI) database (adni.loni.usc.edu). As such, the investigators within the ADNI contributed to the design and implementation of ADNI and/or provided data but did not participate in analysis or writing of this report. A complete listing of ADNI investigators can be found at: http://adni.loni.usc.edu/wp-content/uploads/how_to_apply/ADNI_Acknowledgement_List.pdf. The AIBL study is a consortium between the Commonwealth Scientific and Industrial Research Organisation (CSIRO), Edith Cowan University, The Florey Institute and Austin Health. Partial financial support was provided by the US Alzheimer's Association, the Alzheimer's Drug Discovery Foundation, an anonymous foundation, the Cooperative Research Centre for Mental Health, the CSIRO Science and Industry Endowment Fund, the Dementia Collaborative Research Centres, the Victorian Government Operational Infrastructure Support program, the Australian Alzheimer's Research Foundation, the National Health and MRC and the Yulgilbar Foundation.

Appendix A. Supplementary data

Supplementary data related to this article can be found at https://doi.org/10.1016/j.eclinm.2023.102247.

References

1 Apostolova LG. Alzheimer disease. *Continuum*. 2016;22:419–434.
2 Nestor PJ, Scheltens P, Hodges JR. Advances in the early detection of Alzheimer's disease. *Nat Med*. 2004;10(Suppl):S34–S41.
3 Hampel H, Bürger K, Teipel SJ, Bokde ALW, Zetterberg H, Blennow K. Core candidate neurochemical and imaging biomarkers of Alzheimer's disease. *Alzheimers Dement*. 2008;4:38–48.
4 Duyckaerts C, Delatour B, Potier M-C. Classification and basic pathology of Alzheimer disease. *Acta Neuropathol*. 2009;118:5–36.
5 Ewers M, Sperling RA, Klunk WE, Weiner MW, Hampel H. Neuroimaging markers for the prediction and early diagnosis of Alzheimer's disease dementia. *Trends Neurosci*. 2011;34:430–442.
6 Murray ME, Graff-Radford NR, Ross OA, Petersen RC, Duara R, Dickson DW. Neuropathologically defined subtypes of Alzheimer's disease with distinct clinical characteristics: a retrospective study. *Lancet Neurol*. 2011;10:785–796.
7 Illakiya T, Karthik R. Automatic detection of Alzheimer's Disease using deep learning models and neuro-imaging: current trends and future perspectives. *Neuroinformatics*. 2023;21:339–364.

8 Qin Z, Liu Z, Guo Q, Zhu P. 3D convolutional neural networks with hybrid attention mechanism for early diagnosis of Alzheimer's disease. *Biomed Signal Process Control*. 2022;77:103828.
9 Ahmed HM, Elsharkawy ZF, Elkorany AS. Alzheimer disease diagnosis for magnetic resonance brain images using deep learning neural networks. *Multimed Tools Appl*. 2023;82:17963–17977. https://doi.org/10.1007/s11042-022-14203-1.
10 Thayumanasamy I, Ramamurthy K. Performance analysis of machine learning and deep learning models for classification of Alzheimer's disease from brain MRI. *Trait Du Signal*. 2022;39:1961–1970.
11 van der Haar D, Moustafa A, Warren SL, Alashwal H, van Zyl T. An Alzheimer's disease category progression sub-grouping analysis using manifold learning on ADNI. *Sci Rep*. 2023;13:10483.
12 Sharma R, Goel T, Tanveer M, Murugan R, FDN-ADNet. Fuzzy LS-TWSVM based deep learning network for prognosis of the Alzheimer's disease using the sagittal plane of MRI scans. *Appl Soft Comput*. 2022;115:108099.
13 Illakiya T, Ramamurthy K, Siddharth MV, Mishra R, Udainiya A. AHANet: adaptive hybrid attention network for Alzheimer's disease classification using brain magnetic resonance imaging. *Bioengineering (Basel)*. 2023;10:714. https://doi.org/10.3390/bioengineering10060714.
14 Mirabnahrazam G, Ma D, Beaulac C, et al. Predicting time-to-conversion for dementia of Alzheimer's type using multi-modal deep survival analysis. *Neurobiol Aging*. 2023;121:139–156.
15 Nakagawa T, Ishida M, Naito J, et al. Prediction of conversion to Alzheimer's disease using deep survival analysis of MRI images. *Brain Commun*. 2020;2:fcaa057.
16 Li H, Habes M, Wolk DA, Fan Y. Alzheimer's Disease Neuroimaging Initiative and the Australian Imaging Biomarkers and Lifestyle Study of Aging. A deep learning model for early prediction of Alzheimer's disease dementia based on hippocampal magnetic resonance imaging data. *Alzheimers Dement*. 2019;15:1059–1070.
17 Young AL, Marinescu RV, Oxtoby NP, et al. Uncovering the heterogeneity and temporal complexity of neurodegenerative diseases with Subtype and Stage Inference. *Nat Commun*. 2018;9:4273.
18 Yang Z, Nasrallah IM, Shou H, et al. A deep learning framework identifies dimensional representations of Alzheimer's Disease from brain structure. *Nat Commun*. 2021;12:7065.
19 Goodfellow I, Pouget-Abadie J, Mirza M, et al. Generative adversarial networks. *Commun ACM*. 2020;63:139–144.
20 Li Y, Yang T, Zhou J, Ye J. Multi-task learning based survival analysis for predicting Alzheimer's disease progression with multi-source block-wise missing data. In: *Proceedings of the 2018 SIAM international conference on data mining*. Philadelphia, PA: Society for Industrial and Applied Mathematics; 2018:288–296.
21 Ghazi MM, Nielsen M, Pai A, et al. Robust training of recurrent neural networks to handle missing data for disease progression modeling. *arXiv*; 2018 [cs.CV] http://arxiv.org/abs/1808.05500.
22 Klein JP, Moeschberger ML. *Survival analysis*. Springer New York; 2023.
23 Kay R. Proportional hazard regression models and the analysis of censored survival data. *J R Stat Soc Ser C Appl Stat*. 1977;26:227.
24 Petersen RC, Aisen PS, Beckett LA, et al. Alzheimer's disease neuroimaging initiative (ADNI): clinical characterization. *Neurology*. 2010;74:201–209.
25 Mueller SG, Weiner MW, Thal LJ, et al. Ways toward an early diagnosis in Alzheimer's disease: the Alzheimer's disease neuroimaging initiative (ADNI). *Alzheimers Dement*. 2005;1:55–66.
26 Mueller SG, Weiner MW, Thal LJ, et al. The Alzheimer's disease neuroimaging initiative. *Neuroimaging Clin N Am*. 2005;15:869–877. xi–xii.
27 Fischl B. FreeSurfer. *Neuroimage*. 2012;62:774–781.
28 Destrieux C, Fischl B, Dale A, Halgren E. Automatic parcellation of human cortical gyri and sulci using standard anatomical nomenclature. *Neuroimage*. 2010;53:1–15.
29 Xuan G, Zhang W, Chai P. EM algorithms of Gaussian mixture model and hidden Markov model. In: *Proceedings 2001 international conference on image processing (cat. No.01CH37205)*. IEEE; 2002. https://doi.org/10.1109/icip.2001.958974.
30 Kingma DP, Welling M. Auto-encoding variational bayes. *arXiv*; 2013 [stat.ML] http://arxiv.org/abs/1312.6114.
31 Lin DY. Non-parametric inference for cumulative incidence functions in competing risks studies. *Stat Med*. 1997;16:901–910.
32 Kingma DP, Ba J. Adam: A Method for Stochastic Optimization. *arXiv*; 2014 [csLG] https://arxiv.org/abs/1412.6980.
33 Emdin CA, Khera AV, Kathiresan S. Mendelian randomization. *JAMA*. 2017;318:1925–1926.
34 Bush WS, Moore JH. Chapter 11: genome-wide association studies. *PLoS Comput Biol*. 2012;8:e1002822.
35 Hayes B. Overview of statistical methods for genome-wide association studies (GWAS). *Methods Mol Biol*. 2013;1019:149–169.
36 Burgess S, Bowden J. Integrating summarized data from multiple genetic variants in Mendelian randomization: bias and coverage properties of inverse-variance weighted methods. *arXiv*; 2015 [stat.AP] http://arxiv.org/abs/1512.04486.
37 Verbanck M, Chen C-Y, Neale B, Do R. Publisher Correction: detection of widespread horizontal pleiotropy in causal relationships inferred from Mendelian randomization between complex traits and diseases. *Nat Genet*. 2018;50:1196.
38 Hemani G, Bowden J, Davey Smith G. Evaluating the potential role of pleiotropy in Mendelian randomization studies. *Hum Mol Genet*. 2018;27:R195–R208.
39 Burgess S, Thompson SG. Interpreting findings from Mendelian randomization using the MR-Egger method. *Eur J Epidemiol*. 2017;32:377–389.
40 Campbell MR, Ashrafzadeh-Kian S, Petersen RC, et al. P-tau/Aβ42 and Aβ42/40 ratios in CSF are equally predictive of amyloid PET status. *Alzheimers Dement (Amst)*. 2021;13:e12190.
41 Li K, Chan W, Doody RS, Quinn J, Luo S, Alzheimer's Disease Neuroimaging Initiative. Prediction of conversion to Alzheimer's disease with longitudinal measures and time-to-event data. *J Alzheimers Dis*. 2017;58:361–371.
42 Cox DR. Regression models and life-tables. *J R Stat Soc*. 1972;34:187–202.
43 Brentnall AR, Cuzick J. Use of the concordance index for predictors of censored survival data. *Stat Methods Med Res*. 2018;27:2359–2373.
44 Li Y, Cao K, Zhu G, et al. Genomic analyses of an extensive collection of wild and cultivated accessions provide new insights into peach breeding history. *Genome Biol*. 2019;20:36.
45 Setti SE, Reed MN. Network activity changes in the pathophysiology of Alzheimer's disease: the role of aging and early entorhinal cortex dysfunction. *Metab Brain Dis*. 2022;37:289–298.
46 Guzman VA, Carmichael OT, Schwarz C, et al. White matter hyperintensities and amyloid are independently associated with entorhinal cortex volume among individuals with mild cognitive impairment. *Alzheimers Dement*. 2013;9:S124–S131.
47 Ma D, Fetahu IS, Wang M, et al. The fusiform gyrus exhibits an epigenetic signature for Alzheimer's disease. *Clin Epigenetics*. 2020;12:129.
48 Tang Y, Yan Y, Mao J, Ni J, Qing H. The hippocampus associated GABAergic neural network impairment in early-stage of Alzheimer's disease. *Ageing Res Rev*. 2023;86:101865.
49 Mu Y, Gage FH. Adult hippocampal neurogenesis and its role in Alzheimer's disease. *Mol Neurodegener*. 2011;6:85.
50 Payami H, Zareparsi S, Montee KR, et al. Gender difference in apolipoprotein E-associated risk for familial Alzheimer disease: a possible clue to the higher incidence of Alzheimer disease in women. *Am J Hum Genet*. 1996;58:803–811.
51 Poulakis K, Pereira JB, Mecocci P, et al. Heterogeneous patterns of brain atrophy in Alzheimer's disease. *Neurobiol Aging*. 2018;65:98–108.
52 Silva MVF, Loures C de MG, Alves LCV, de Souza LC, Borges KBG, Carvalho M das G. Alzheimer's disease: risk factors and potentially protective measures. *J Biomed Sci*. 2019;26:33.
53 Florean I, Penolazzi B, Menichelli A, et al. Using the ATN system as a guide for the neuropsychological assessment of Alzheimer's disease. *J Clin Exp Neuropsychol*. 2021;43:926–943.
54 Grøntvedt GR, Lauridsen C, Berge G, et al. The amyloid, tau, and neurodegeneration (A/T/N) classification applied to a clinical research cohort with long-term follow-up. *J Alzheimers Dis*. 2020;74:829–837.
55 Ossenkoppele R, Pichet Binette A, Groot C, et al. Amyloid and tau PET-positive cognitively unimpaired individuals are at high risk for future cognitive decline. *Nat Med*. 2022;28:2381–2387.

56 Gatz M, Reynolds CA, Fratiglioni L, et al. Role of genes and environments for explaining Alzheimer disease. *Arch Gen Psychiatry*. 2006;63:168–174.

57 Barber RC. The genetics of Alzheimer's disease. *Scientifica (Cairo)*. 2012;2012:246210.

58 Hong S, Prokopenko D, Dobricic V, et al. Genome-wide association study of Alzheimer's disease CSF biomarkers in the EMIF-AD Multimodal Biomarker Discovery dataset. *Transl Psychiatry*. 2020;10:403.

59 Shi J, Potash JB, Knowles JA, et al. Genome-wide association study of recurrent early-onset major depressive disorder. *Mol Psychiatry*. 2011;16:193–201.

60 Winham SJ, Cuellar-Barboza AB, Oliveros A, et al. Genome-wide association study of bipolar disorder accounting for effect of body mass index identifies a new risk allele in TCF7L2. *Mol Psychiatry*. 2014;19:1010–1016.

61 Poulakis K, Pereira JB, Muehlboeck J-S, et al. Multi-cohort and longitudinal Bayesian clustering study of stage and subtype in Alzheimer's disease. *Nat Commun*. 2022;13:4566.

62 Whitwell J, Martin PR, Graff-Radford J, et al. Investigating heterogeneity and neuroanatomic correlates of longitudinal clinical decline in atypical Alzheimer disease. *Neurology*. 2022;98(24):e2436–e2445. https://doi.org/10.1212/WNL.0000000000200336.